water

MDPI

Article

Linkage between Granite Weathering and Gully Erosion in Subtropical Region

Shu Zhang [1], Yong Zhang [2], Gang Huang [3], Bo Zhang [4], Yichan Li [2], Xin Chen [5], Junkang Xu [5] and Yujie Wei [5,*]

[1] Changjiang Institute of Survey Planning Design and Research, Wuhan 430010, China
[2] Yangtze River Basin Monitoring Center Station for Soil and Water Conservation, Changjiang Water Resources Commission, Wuhan 430010, China
[3] Sichuan Energy Power Development Group Company Ltd., Chengdu 610041, China
[4] Guangxi Nuclear Power Company Ltd., Fangchenggang 538004, China
[5] College of Resources and Environment, Huazhong Agricultural University, Wuhan 430070, China
* Correspondence: wyj@mail.hzau.edu.cn; Fax: +86-27-87288249

Abstract: Granites, widely distributed in the Earth's crust, undergo pedogenic processes, shaping diverse soil-mantled landscapes influenced by climatic factors in different regions. Investigating the geochemical signatures in granite weathering profiles across varying climatic conditions provides valuable insights into the intricate interplay between weathering and landscape evolution. In this study, the geochemical features, particularly major and rare earth elements, and the weathering degree of granites across temperate to subtropical regions in China were examined. The results indicated significant variations in the geochemical characteristics of granite weathering profiles, both at a pedon and regional scale ($p < 0.01$). With increasing hydrothermal conditions from north to south, soil pH shifted from neutral to acidic, accompanied by the leaching of major elements (K_2O, Na_2O, CaO, and MgO) and the enrichment of Al and Fe. The total rare earth elements (∑REEs) ranged from 75 to 352 ppm, and light rare earth elements (LREEs) from 71 to 317 ppm, exhibiting less significant variations across the study area, while heavy rare earth elements (HREEs) showed higher concentrations in the subtropical region (3 to 35 ppm). Plagioclases dominated the weathering process in temperate regions, with K-feldspar progressively increasing and, eventually, dominating from temperate to subtropic regions, resulting in a shift in clay minerals from 2:1-type in the temperate to 1:1-type in the subtropic. The chemical index of alteration (CIA) and comprehensive weathering index (W) increased from fresh rock to residual soils along the weathering profiles and from north to south across the study area, ranging from 50.72 to 97.44 and 35.11 to 70.62, respectively. The intensified granite weathering degree was significantly influenced by climatic conditions ($p < 0.05$), especially the multi-year average precipitation (22.4%) and relative humidity (9.1%) ($p < 0.01$). Gully erosion on the granite weathering mantle was concentrated in granites with a comprehensive weathering index exceeding 52.51, and the spatial variation of the granite weathering degree aligned with the spatial distribution of gully density across the study area.

Keywords: chemical weathering; granite weathering profile; gully erosion; climatic gradient

Citation: Zhang, S.; Zhang, Y.; Huang, G.; Zhang, B.; Li, Y.; Chen, X.; Xu, J.; Wei, Y. Linkage between Granite Weathering and Gully Erosion in Subtropical Region. *Water* **2024**, *16*, 751. https://doi.org/10.3390/w16050751

Academic Editor: Barry T. Hart

Received: 22 January 2024
Revised: 23 February 2024
Accepted: 28 February 2024
Published: 1 March 2024

1. Introduction

Chemical weathering is a pivotal process in providing essential nutrients to ecosystems and regulating the Earth's surface environment over geological time [1]. The onset of chemical weathering is initiated by the intricate interplay among rock, water, and the atmosphere [2]. This process is governed by various factors, including mineral geochemistry, temperature, environment, and topography [3]. Granite covers approximately 9% of the land in China, with an expansive area of up to 800,000 km^2 [4], particularly distributed in the southern regions of China [5]. Research on granite residual soil spans various scales, from morphological microscopes [6] to weathering under diverse climatic, geomorphic, and

topography conditions [7–9]. Petrography, mineralogy, geochemistry, and micromorphology are employed in these studies. Significant progress has been attained in comprehending the weathering dynamics of residual granite soil. This progress encompasses various facets, such as the exploration of microcosmic properties and the disintegration of granite from both geotechnical and geological engineering perspectives [10–12]. Additionally, investigations have delved into the amalgamation of mineralogical, chemical, and biological conditions associated with the heterogeneity of the granite weathering mantle [13–17]. This includes the formation, migration, and enrichment of secondary minerals and various elements. Therefore, a study on granite weathering would facilitate a better understanding of the formation mechanism of gully erosion [18].

In southern China, the granite weathering rate experiences a notable escalation influenced by elevated temperatures and humidity levels, providing abundant materials for gully erosion [19]. The thick weathering mantle has been regarded as the prerequisite for the development of this gully with a large dimensional scale [20]. Additionally, this type of gully erosion exhibits distinctive characteristics, such as rapid expansion, severe soil loss, extensive damage, and intricate combined erosion patterns [21]. According to the 2005 National Survey on Soil and Water Loss, more than 2.39×10^5 gullies, with an annual erosion rate exceeding 500,000 t km^{-2} yr^{-1} and covering an area of 1.22×10^5 ha, were distributed across seven provinces (Hubei, Hunan, Jiangxi, Anhui, Fujian, Guangdong, and Guangxi) in southern China [22], and it has been reported that these gullies caused the destruction, burial, or abandonment of 380,000 hectares of cultivated land, resulting in a direct economic loss of CNY 550 million from 1949 to 2005 [23]. Due to these facts, gully erosion concentrated in granite weathering mantles has emerged as a significant national concern in recent decades [24].

To achieve effective control of gully erosion in southern China, researchers have increasingly focused on studying the erosion process and formation mechanism of these gullies [20]. The prevailing consensus is that the thick granite weathering mantle, characterized by distinctive soil structures and physic-mechanical properties, serves as an internal prerequisite for this gully erosion [25–34]. Meanwhile, external factors, such as abundant precipitation and high temperatures, which drive the weathering process, play a significant role in its formation [19,22,24]. On a regional scale, the spatial distribution of these gullies exhibits a notable zonal characteristic, aligning parallel to the coastline of southern China. This distribution pattern is strongly influenced by humid and thermal conditions, which play a pivotal role in the formation of gullies [35]. At the watershed or catchment scale, factors such as the slope gradient, slope aspect, and altitude or elevation are pivotal for the formation of these gullies [10,21]. At a pedon/plot scale, certain factors, such as soil texture [36,37], cements [30], structure [38], moisture [39], shear strength [40], and anti-erosion ability [31], have been identified as the determinants influencing these gullies. While it is widely acknowledged that granite weathering plays a pivotal role in shaping the spatial variability of granitic soil properties, limited research works have delved into the relationship between granite weathering and gully erosion.

According to the above-mentioned background, this study is centered on the vertical stratification and zonal distribution of granite residual soil. We explore the evolutionary characteristics of the granite weathering process and elucidate the impact of chemical weathering on gully erosion through the measurement and calculation of chemical element migration, weathering degree index, and other relevant parameters. This approach enhances our understanding of the material composition and development of collapsing gully erosion.

2. Materials and Methods

2.1. Study Sites and Sample Collection

Granite weathering profiles developed from the same parent rocks were selected from areas with a climatic gradient: from Fushun County (41°53′ N, 124°01′ E~41°62′ N, 124°10′ E, Liaoning Province, China) to Wuhua County (24°06′ N, 115°36′ E~24°13′ N,

115°34′ E, Guangdong Province, China). Across the study area, the mean annual temperature and precipitation ranged from 9.2 to 22.0 °C and from 493 to 1700 mm, respectively, indicating an escalating trend in hydrothermal conditions from north to south. The average condition of the climate in the recent five years is summarized in Table 1. This climatic variation contributes to the spatial heterogeneity observed in desilication and allitization across the study area. A field investigation indicated a progressive increase in the depth of granite weathering profiles throughout the study area. In the temperate region, this depth remained below 5 m, whereas, in the subtropical region, it spanned from ten to a hundred meters. The granite weathering profiles were categorized into two segments: residual soils, further subdivided into eluvial (A), illuvium (B), and parent material horizons (C); and weathered rocks, further subdivided into moderately weathered (MW), highly weathered (HW), and fresh rock (R) horizons. In the temperate region, where the weathering mantle had limited thickness, the granite weathering profiles were categorized into four horizons: A, B, C, and R. All selected granite weathering profiles were situated under similar topographical conditions and land use. Additional details about the study area and soils are presented in Figure 1 and Table 1.

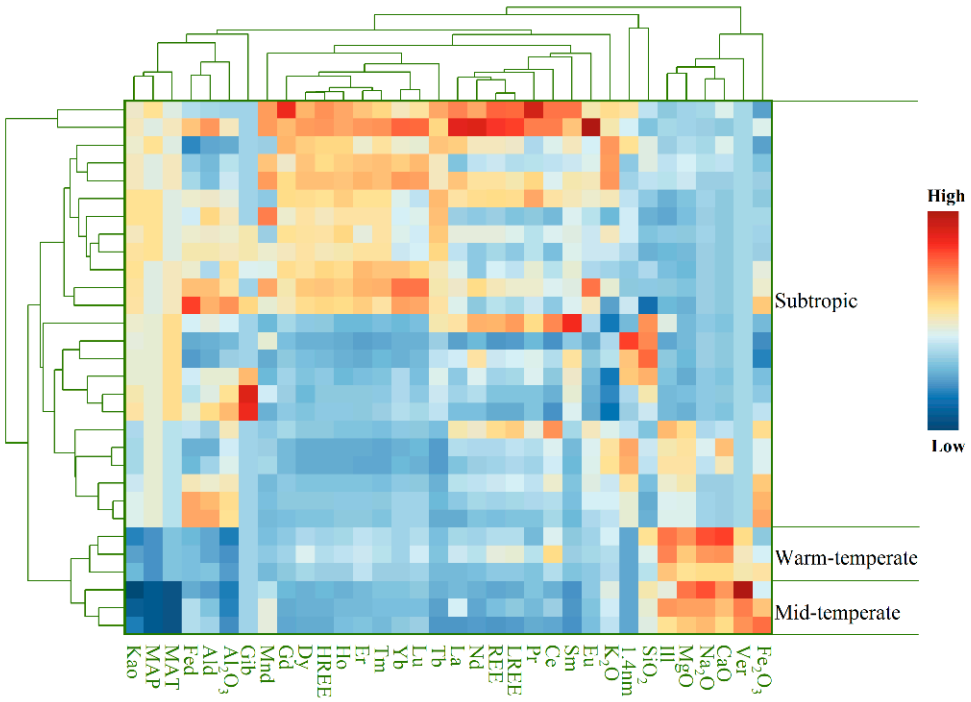

Figure 1. Heatmap of soil properties, geochemical elements, and environmental factors, normalization of raw data using Z-score method, $x' = \frac{x-\mu}{\delta}$; μ, the average of raw data; δ, the standard deviation of raw data. (*i*) MAP and MAT, mean annual precipitation and temperature. (*ii*) SiO_2, Al_2O_3, Fe_2O_3, CaO, MgO, K_2O, and Na_2O, the content of major earth elements SiO_2, Al_2O_3, Fe_2O_3, CaO, MgO, K_2O, and Na_2O; La, Ce, Pr, Nd, Sm, Eu, Gd, Tb, Dy, Ho, Er, Tm, Yb, and Lu, the content of rare earth elements La, Ce, Pr, Nd, Sm, Eu, Gd, Tb, Dy, Ho, Er, Tm, Yb, and Lu; ∑REE, the sum of 14 REE; LREE, the sum of light REE; HREE, the sum of heavy REE; L/H, the ratio of LREE and HREE.

Table 1. Climatic factors (average values from 2018 to 2024) across the study area.

Climatic Factor	FS	LY	TC	GX	CT	WH
T_{max} (°C)	31	33	35	36	36	34
T_{min} (°C)	−15	−5	0	6	7	13
T_{CI}	8	7	6	5	4	4
T_{CV} (%)	1	1	1	0	0	0
$T_{(max\text{-}min)}$ (°C)	46	38	35	30	29	21

Table 1. *Cont.*

Climatic Factor	FS	LY	TC	GX	CT	WH
$T_{average}$ (°C)	9	15	17	21	21	24
T_{std} (°C)	13	10	9	8	7	5
P_{max} (mm)	307	305	336	272	296	340
P_{min} (mm)	1	1	11	7	9	8
P_{CI}	57	62	68	58	61	77
P_{CV} (%)	1	2	1	1	1	1
$P_{(max\text{-}min)}$ (mm)	306	304	325	265	287	332
$P_{average}$ (mm)	70	64	117	110	120	117
P_{std} (mm)	89	93	106	92	94	115
$RH_{average}$ (%)	61	66	77	74	77	74
RH_{min} (%)	8	10	15	15	12	17

Note: T, P, and RH are the temperature, precipitation, and relative humility, respectively; max, min, CI, CV, (max–min), average, std in subscripts are the maximum, minimum, confidence interval, coefficient of variation, temperature difference between the maximum and minimum value, average value, and standard deviation, respectively.

The collection of experimental samples from each site followed a randomized block design with four field replicates. Composited and undisturbed core samples (100 cm^3) were obtained from each horizon; the composited soils were collected from each horizon using an S-shaped sampling strategy and stored in rigid plastic boxes to prevent soil structure disturbance. After thorough air-drying at room temperature, the pretreated soil samples were analyzed using standardized methods (Table 2).

Table 2. Descriptive statistics of soil properties in different climate zones.

	Climate	Mean	std	CV (%)	Max	Min	Kurtosis	Skewness	Climate	Mean	std	CV (%)	Max	Min	Kurtosis	Skewness
Clay (%)	Temperate	20	5	37	31	11	−0.6	0.6	Subtropic	28	3	43	49	11	−0.3	0.3
Silt (%)		25	4	46	42	10	−0.7	0.2		30	5	24	45	18	−0.6	0.4
Sand (%)		55	6	18	73	43	0.2	0.1		42	4	29	65	19	−0.3	−0.1
pH		6.1	0.8	13.8	7.1	4.9	−0.1	−0.3		5.1	0.6	10.9	6.2	4.1	−0.6	0.5
SOM (g/kg)		9.8	13.4	13.2	36.7	2.1	5.4	2.3		9.1	4.8	52.8	19.5	2.4	−0.8	0.5
CEC (cmol/kg)		10.3	4.2	40.9	16.3	4.1	0.2	−0.1		22.6	6.7	29.7	32.8	9.5	−0.7	−0.4
Kao (%)		31	14.9	48.3	48	8	−0.6	−0.6		80	9.3	11.7	91	60	0.1	−0.9
Ill (%)		33	8.5	25.4	42	20	−0.9	−0.7		13	8.0	63.6	33	3	0.5	1.0
Ver (%)		36	20.5	57.4	72	17	1.2	1.2		N/A	N/A	N/A	N/A	N/A	N/A	N/A
1.4 nm (%)		N/A	N/A	N/A	N/A	N/A	N/A	N/A		7	4.7	64.4	20	1	0.5	1.0
Gib (%)		N/A	N/A	N/A	N/A	N/A	N/A	N/A		1	1.0	193.0	4	0	3.6	2.1
Fe_d (g/kg)		10.9	2.6	23.8	14.2	8.1	−1.8	0.6		17.8	8.1	45.3	37.5	4.6	0.1	0.5
Al_d (g/kg)		2.1	0.6	28.5	3.0	1.5	−1.8	0.4		4.4	1.9	43.8	7.6	1.7	−1.3	0.1
Mn_d (g/kg)		0.3	0.2	70.3	0.6	0.1	−2.2	0.4		0.5	0.4	90.8	1.2	0.0	−1.0	0.8

Note: SOM, soil organic material; CEC, cation exchange capacity; Fe_d, Al_d, and Mn_d, free iron, aluminum, and manganese oxides; mean, std, CV, Max, and Min are average value, standard deviation, coefficient of variation, and maximum and minimum values, respectively.

2.2. Determination of Geochemical Elements

Major elements, mainly including SiO_2, Al_2O_3, Fe_2O_3, CaO, MgO, K_2O, Na_2O, P_2O_5, TiO_2, and MnO, were determined using the anhydrous lithium tetraborate melting method with an X-ray fluorescence (XRF) spectrometer (Axios, PANalytical, Almelo, The Netherlands) [41]. Rare earth elements (REEs) were analyzed through inductively coupled plasma mass spectrometry (ICP-MS, NexION 350X, PerkinElmer, Waltham, Massachusetts, USA) for all soil samples [42]. A regular foreign sample and a blank data quality management sample were used. In this study, the chondrite proposed by Sun and McDonough [43] was used to standardize the REEs (~10^{-6}) to remove the odd–even effect, and ∑REEs, LREEs, HREEs, L/H, δEu, and δCe were used to characterized the REEs. Specifically, the ∑REEs were the sum of all the identified REEs; LREEs were the sum of the light REEs, including

La, Ce, Pr, Nd, Sm, and Eu; the HREEs were the sum of the heavy REEs, including Gd, Tb, Dy, Ho, Er, Tm, Yb, and Lu; L/H was the ratio of LREEs and HREEs. δEu and δCe, respectively, indicated the abnormality degree of Eu and Ce and were calculated with Equations (1) and (2):

$$\delta\mathrm{Eu} = \frac{\mathrm{Eu}_N}{(\mathrm{Sm}_N + \mathrm{Gd}_N)/2} \quad (1)$$

$$\delta\mathrm{Ce} = \frac{\mathrm{Ce}_N}{(\mathrm{La}_N + Pr_N)/2} \quad (2)$$

where the subscript *N* represents chondrite normalization.

2.3. Element Migration Rate

The element migration rate was determined by analyzing the concentration variations of major elements in different horizons [44]. Herein, Al was selected as the relatively stable element and the migration rate ($\tau_{i,j}$) was calculated with Equation (3) [45]:

$$\tau_{i,j} = \left(\frac{\mathrm{C_{j,w}}/\mathrm{C}_{i,w}}{\mathrm{C}_{j,p}/\mathrm{C}_{i,p}} - 1 \right) \times 100 \quad (3)$$

where C, the concentration of the element; *i* and *j*, the stable and moveable elements, respectively; *w* and *p*, the weathering layer and fresh rock layer, respectively. The $\tau_{i,j} > 0$ indicates the enrichment of the element compared to the fresh rock. Conversely, τi,j < 0 means the element was leached from the fresh rock. When τi,j = 0, the element remained stable, indicating neither enrichment nor leaching.

2.4. Evaluation of Weathering Degree

The chemical index of alteration (CIA) [46] was adopted to quantify the weathering degree:

$$\mathrm{CIA} = [\mathrm{Al_2O_3}/(\mathrm{Al_2O_3} + \mathrm{CaO^*} + \mathrm{K_2O} + \mathrm{Na_2O})] \times 100 \quad (4)$$

where CaO*, CaO in silicate excluded carbonate and phosphate. The molar ratio was employed for the determination of each oxide. Nevertheless, the CIA can only distinguish weathering stages, and for a quantitative definition of the degree of weathering in each section, it was necessary to consider the influence of the parent rock as well as the climatic conditions [3]. As different types of granite contain various rock-forming minerals with different weathering resistances, a comprehensive weathering index (W) was adopted in this paper to characterize the weathering degree of each section. The index expression was relative to the parent rock wetness, providing insight into the geochemical process of weathering and common properties across various lithologies [1].

$$\mathrm{W} = \left[1 - \left(\frac{\mathrm{E}' \times \bar{\mathrm{t}} + \mathrm{E}}{2} \right) \right] \times 100\% \quad (5)$$

where $\bar{\mathrm{t}}$, the average leaching coefficient of five oxides (SiO_2, CaO, MgO, K_2O, and Na_2O); E, the equilibrium degree of the variation coefficient of seven oxides (SiO_2, Al_2O_3, Fe_2O_3, CaO, MgO, K_2O, and Na_2O); and E′, the equilibrium degree of seven weathering rates (SiO_2/Al_2O_3, SiO_2/Fe_2O_3, $Al_2O_3/R(Al_2O_3)$, $Fe_2O_3/R(Fe_2O_3)$, Fe_2O_3/Al_2O_3, Al_2O_3/Fe_2O_3, and $(Al_2O_3 + Fe_2O_3)/SiO_2$); $R(Al_2O_3)$ and $R(Fe_2O_3)$, the content of Al_2O_3 and Fe_2O_3 in the parent rock, respectively. Additionally, the leaching coefficient was calculated as follows:

$$t = \frac{t_1 - t_2}{t_1} \times 100\% \quad (6)$$

$$t_2 = \mathrm{t}' \times \frac{\mathrm{R(Al_2O_3)}}{\mathrm{S(Al_2O_3)}} \times 100\% \quad (7)$$

where t, the migration of oxides from the fresh rock (%); t_1 and t_2, oxides in the fresh rock (%) and oxides under the condition with a consistent Al_2O_3, respectively; t', oxides in the weathering profile (%).

The equilibrium degree (E) was calculated using the following:

$$E = \frac{e^{H(S)}}{S} \quad (8)$$

$$H(s) = -\sum_{i=1}^{s} P_i \cdot \ln P_i \quad (9)$$

where e, Napierian base; H(s), information function; S, number of data; N, sum of series data, and Pi = ni/N.

2.5. Statistical Analysis

The normalization of different dimensional data was carried out using the Z-score method. Normality checks were performed using the Shapiro–Wilk statistics before the analysis. For non-normally distributed results, a natural log transformation was applied, but the raw data were presented in the figures of this article. To depict variations in soil properties and REE distribution among sampling sites, a one-way analysis of variance (ANOVA) was conducted. Pearson's correlation analysis was employed to illustrate the relationship between REE distribution, clay minerals, and soil properties. The impact of environmental factors on soil layers and characteristics of granite weathering was calculated through a redundancy analysis (RDA). Both statistical analyses were carried out using the SPSS software package (version 19.0.0) and OriginPro 2020 was used for figure generation.

3. Results

3.1. Spatial Variation of Granitic Soil Properties

Basic soil properties, mainly including clay mineralogy, particle size distribution, and sesquioxide, were determined for granitic soils in the residual soil horizons. They showed that the soil horizon and climatic gradient contributed significantly to these basic soil properties (Table 2 and Figure 2). The tested soils had an average sand content of 41% (ranging from 15% to 72%) and an average clay content of 20% (ranging from 3% to 49%), indicating a dense texture characteristic of granite residual soil. The sand content decreased from the bottom to the top of the soil profile, while the clay content increased steadily, accompanied by simultaneous increases in the SOM and CEC. The soil pH exhibited noticeable acidification characteristics from bottom to top. The clay fraction in the soil FS and soil LY comprised vermiculite, illite, and kaolinite, with relative contents ranging from 17% to 72%, 20% to 42%, and 8% to 48%, respectively. Along the soil profile, the kaolinite content gradually increased, while vermiculite and illite generally decreased. In the soil profiles from TC to WH, there was a high content of kaolinite, and the clay fractions consisted of kaolinite, illite, and a small amount of 1.4 nm intergrade minerals. Additionally, a small amount of gibbsite was found in the eluvial or illuvial layer of GX, CT, and WH.

A heatmap analysis (Figure 1) demonstrated significant variations in soil properties among the six granite residual soils, with most properties exhibiting significant correlations with the mean annual precipitation and temperature. This indicated the influential role of climate in granite weathering. Across the soil profiles from FS to WH, there was a shift in soil pH from neutral to acidic, indicating an acidification trend along the latitude. The content of free Al_d was lower than that of Fe_d, with an enrichment pattern observed from soil FS to WH for both Fe_d and Al_d. Although there were no significant variations in the SOM and CEC among these residual soils, the soils in the subtropical region exhibited a higher SOM and CEC compared to those in the temperate region. The clay fraction primarily consisted of 2:1-type minerals (vermiculite, illite, and 1.4 nm intergrade mineral) in the temperate, gradually transitioning into 1:1-type minerals (kaolinite) in the subtropic, with

vermiculite and montmorillonite gradually disappearing. Ultimately, the predominant clay mineral type in the soil was mainly kaolinite, with the occasional appearance of gibbsite.

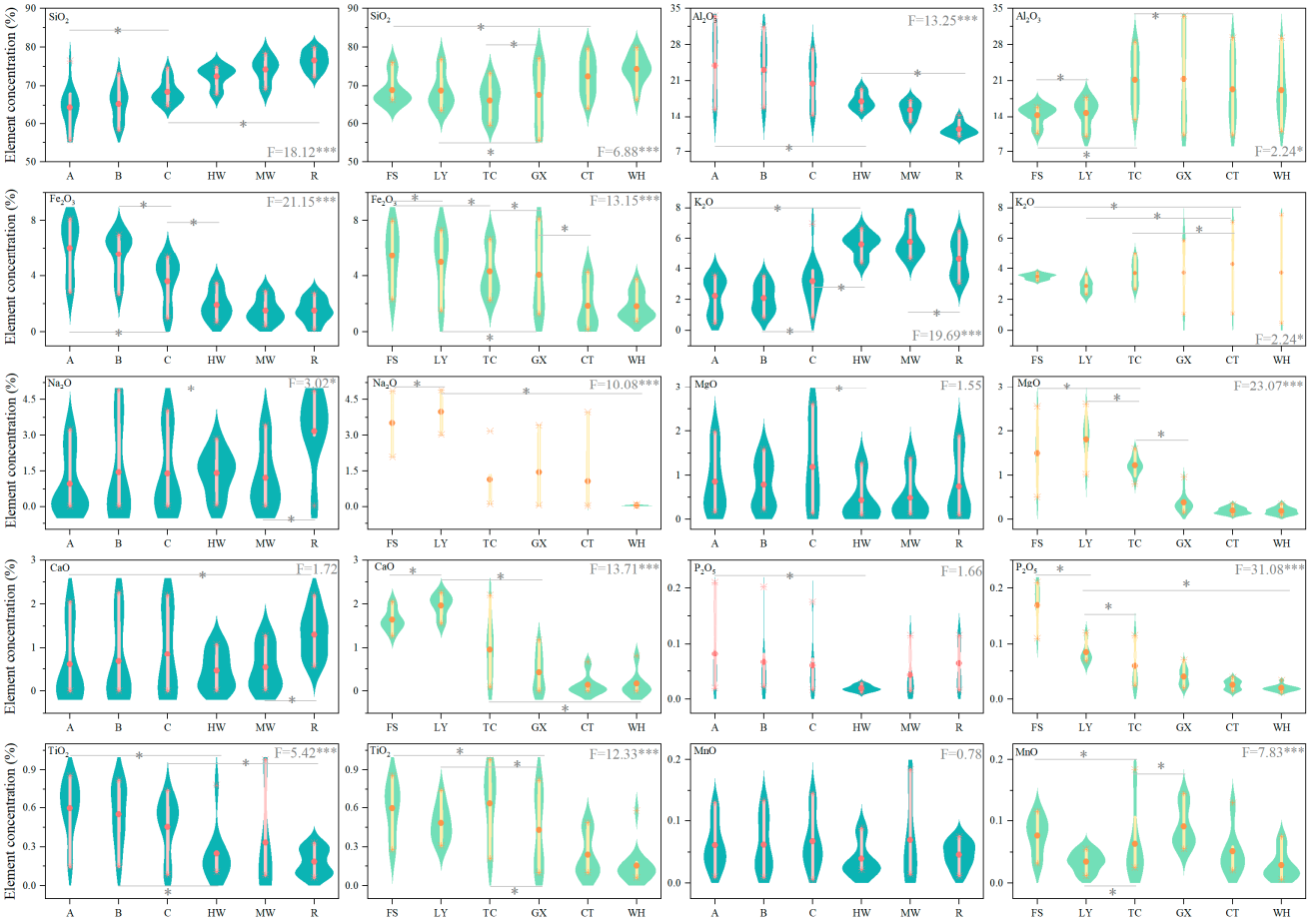

Figure 2. Major element distribution along the granite weathering profile. A, B, C, HW, MW, and R mean eluvial horizon, illuvium horizon, parent horizon in the residual soil layers, highly weathered, moderately weathered, and fresh rock horizon, respectively; FS, LY, TC, GX, CT, and WH represent study sites from Fushun County in Liaoning Province, Lingyi County in Shandong Province, Qichun County in Hubei Province, Ganxian County in Jiangxi Province, Changting County in Fujian Province, Wuhua County in Guangdong Province, respectively; * and *** represent significance at $p < 0.05$ and $p < 0.001$ levels, respectively. The dark and light green colors of the violin plots respectively depict the distribution of elements along the weathering mantle and across the study sites. The area of the violin plots represents the kernel density of the experimental data. The red asterisks (*) at the bottom and top of the box denote the minimum and maximum values of the data, while the red circle (●) inside the box indicates the average value. The pink and yellow boxes represent the interquartile range, encompassing 50% of the data distribution.

3.2. Major Earth Element Migration

Among the granite residual soil profiles, SiO_2, Al_2O_3, and Fe_2O_3 were identified as the main components, constituting 88%, 86%, and 92%, respectively, from soil FS to WH (Figure 2). The content distribution followed the order $SiO_2 > Al_2O_3 > Fe_2O_3$. A consistent variation trend was observed for each major element across the granite residual soils of the six sampling sites. The Al_2O_3 and Fe_2O_3 content increased from the bottom to the top of the profile, while SiO_2, K_2O, Na_2O, MgO, and CaO leached from the parent rock to the upper soil layers. The variance analysis indicated the experience of weathering, the eluviation of base cations, and desilicification–allitization in all profiles, with weathering severity increasing steadily from the parent rock to the surface soil layer.

Comparing the weathering profiles in the temperate and subtropical regions, it was evident that weathering in the subtropical region was more intense, with a larger difference in element leaching and enrichment, particularly in the later stages of the weathering process. Taking the eluvial layer (horizon A) as an example, the average contents of easily migratable K_2O, Na_2O, CaO, and MgO in the subtropical region were 2.5%, 2.7%, 1.0%, and 1.3%, respectively, compared to 2.0%, 0.10%, 0.0%, and 0.4%, respectively, in the temperate region. The contents of K_2O, Na_2O, CaO, and MgO in the subtropical region were significantly lower than those in the temperate region, indicating more leaching and a stronger degree of weathering. Similarly, the comparison of Al_2O_3 and Fe_2O_3 contents in the subtropical and temperate regions showed that the enrichment trend of the Al element in subtropical regions was more pronounced than that in temperate regions.

3.3. Rare Earth Element Migration

The spatial variation of rare earth elements (REEs) in granite weathering profiles across different sampling sites and soil layers is shown in Figure 3. The ∑REEs of soil FS to WH ranged from 91 to 141 ppm, 110 to 207 ppm, 76 to 216 ppm, 97 to 289 ppm, 95 to 277 ppm, and 77 to 248 ppm, respectively. When compared with the parent rock, each soil layer exhibited enrichment in ∑REEs, with the maximal values appearing in the illuvial layer, except for soil CT. The L/H of the six sample sites ranged from 11.9 to 17.4 (mean 14.0), from 8.3 to 12.8 (mean 11.0), from 12.7 to 21.7 (mean 17.7), from 3.7 to 9.0 (mean 5.9), from 4.8 to 8.4 (mean 6.6), and from 12.4 to 24.3 (mean 18.5). δEu ranged from 0.2 to 0.8, and δCe ranged from 0.8 to 1.1. The redistribution of REEs in the soil profiles was a consequence of long-term weathering, resulting in a vertical distinction.

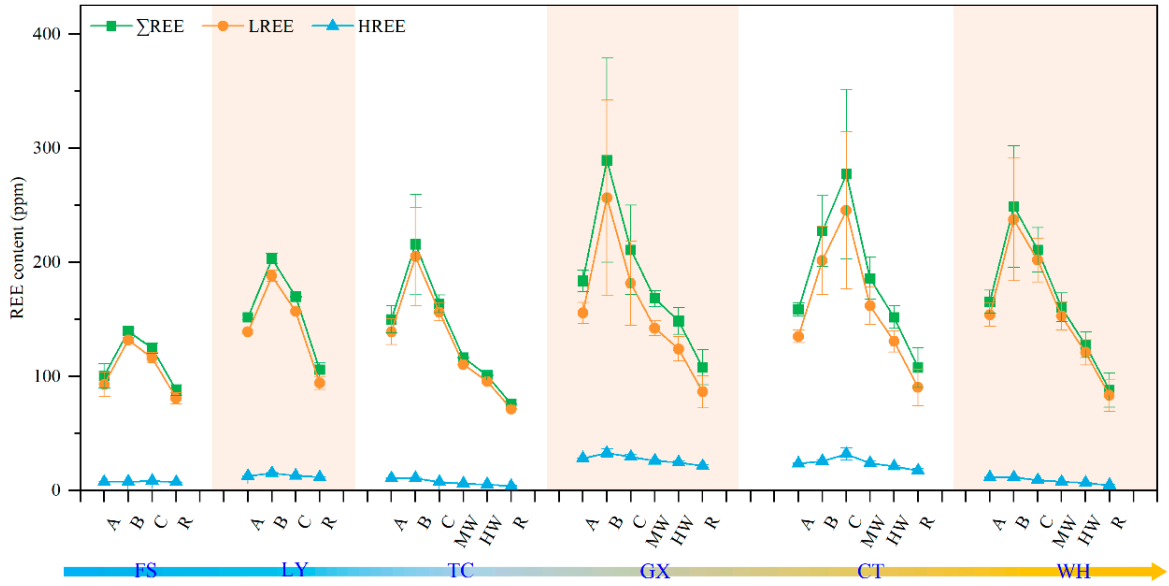

Figure 3. Rare earth element distribution of granite weathering profile across the study area. A, B, C, HW, MW, and R mean eluvial horizon, illuvium horizon, parent horizon in the residual soil layers, highly weathered, moderately weathered, and fresh rock horizon, respectively.

REEs and light rare earth elements (LREEs) showed less significant variations across the study area, while heavy rare earth elements (HREEs), L/H, $(La/Yb)_N$, δEu, and δCe exhibited significant differences. The LRRE enrichment was most evident in all granite residual soil profiles, with the separation of LRREs and HRREs being most visible in the illuvial layer, except for soil CT, showing a similar functionality to La/Yb. The ∑REEs demonstrated the greatest enrichment in the moderate weathered layer, with enrichment coefficients of 1.6, 1.9, 3.3, 3.6, 3.5, and 3.7, respectively. The enrichment coefficient generally improved from north to south across the study area. The redistribution of REEs in the soil profiles was a result of long-term weathering, establishing a vertical distinction.

3.4. Assessment of Granite Weathering Degree

According to the Al_2O_3-CaO + Na_2O-K_2O (A-CN-K) diagram (Figure 4), the evolution of granite weathering in the study area could be classified into three categories: granite weathering profiles in the temperate region (FS and LY) (Figure 4a), granite weathering profiles in TC and WH (Figure 4b), and granite weathering profiles in GX and CT (Figure 4c). The transformation of soil in FS and LY from the parent rock to the residual soil aligned mostly with the $A1_2O_3$–(CaO + Na_2O) line and gradually shifted towards the $A1_2O_3$–K_2O line. This shift suggested that plagioclase weathering was the primary cause for the release of Na and Ca in the temperate region. The variability in TC was comparable to the profiles in the temperate region, but the release amount of Ca and Na was greater, and the leaching layer was even near 0%. Moreover, weathering trends were not fully consistent with the $A1_2O_3$–(CaO + Na_2O) line, indicating that in the process of plagioclase weathering, a small amount of weathering also occurred in potassium feldspar. In the temperate region, granite underwent a phase dominated by plagioclase weathering with leaching of Ca and Na, followed by a period dominated by K-feldspar weathering with a decline in K. In contrast, the intense weathering in the subtropical region compelled a shift in the weathering trend towards the Al element enrichment.

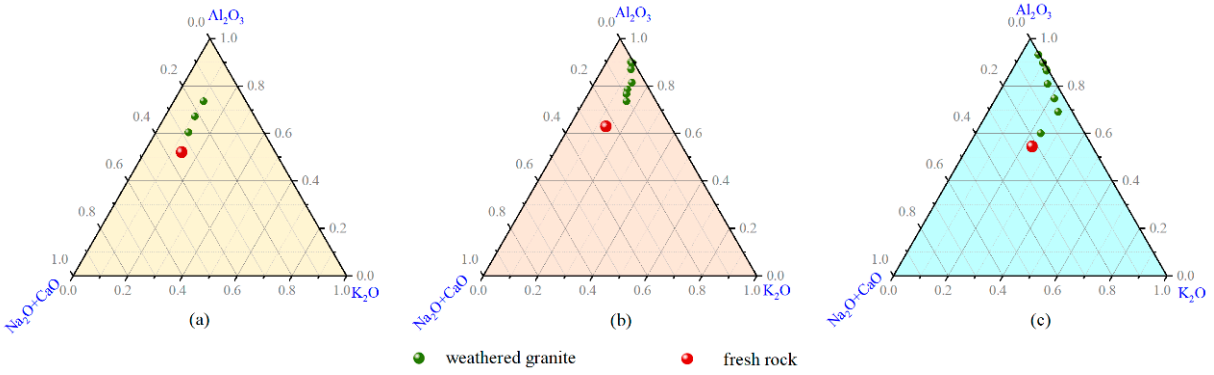

Figure 4. A–CN–K triangle diagram of investigated samples. A, CN, and K are the mole fraction of Al, the sum of the mole fractions of Ca and Na, and the mole fraction of K, respectively. (**a**) granite weathering profiles in the temperate region (FS and LY); (**b**) granite weathering profiles in TC and WH; (**c**) granite weathering profiles in GX and CT.

The chemical index of alteration (CIA) and comprehensive weathering index (W) exhibited a gradual decrease with increasing depth in the granite weathering profiles (Figure 5), signifying a progressive decline in the weathering degree. The CIA for granite residual soil in the temperate region ranged from 50.1 to 69.5, categorizing it as moderately weathered, extending from fresh rock to horizon A. Conversely, subtropical-zone granite residual soil showed a wider range, varying between 50.7 and 97.4. CIA values exceeding 65 in residual soil horizons (A, B, and C) indicated a strongly weathered state. Notably, the coefficient of variation for the CIA in the subtropical region exhibited more significant variations (0.2~18.7) compared to the temperate region. In addition, similar trends were observed for the W values, suggesting common parent rock sources for these weathering profiles. Moreover, most of the considered climatic factors had significant correlations with the CIA and W ($p < 0.05$) (Figure 6a). Among these factors, multiple-year average precipitation (22.4%) and relative humidity (9.1%) had the predominant contribution ($p < 0.01$) to the granite weathering degree (Figure 6b). In general, both the CIA and W consistently increased from the fresh rock to the residual soil horizon and displayed a north-to-south increase across the study area. The spatial variation of the granite weathering degree was primarily determined by the comprehensive effects of temperature and precipitation (Figure 6c).

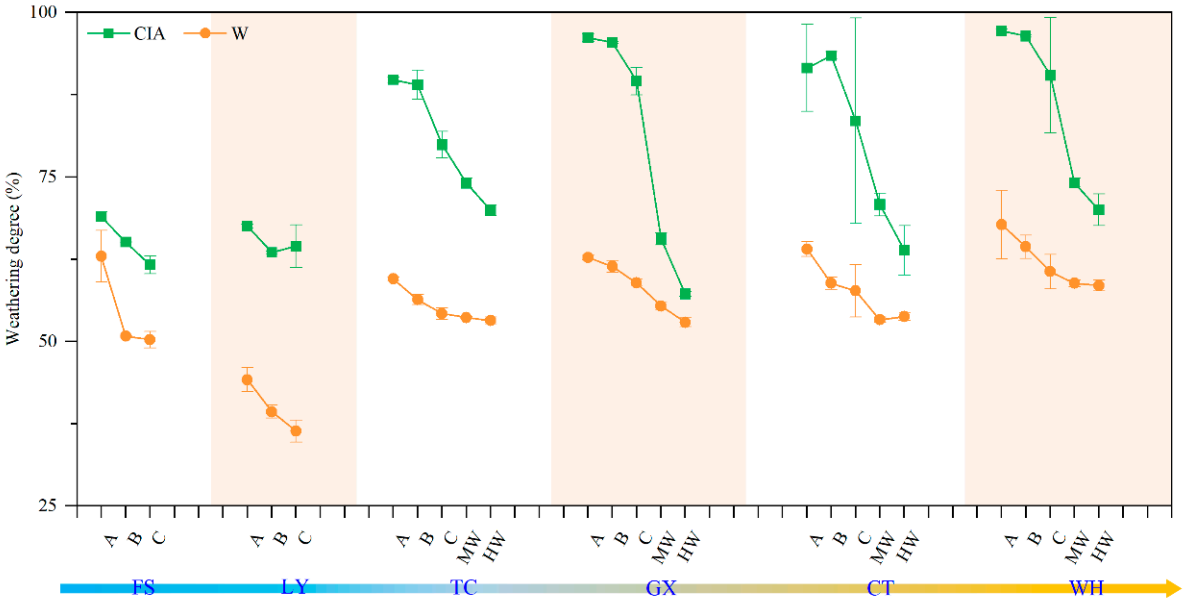

Figure 5. Weathering degree of investigated samples across the study area. A, B, C, HW, MW, and R mean eluvial horizon, illuvium horizon, parent horizon in the residual soil layers, highly weathered, moderately weathered, and fresh rock horizon, respectively.

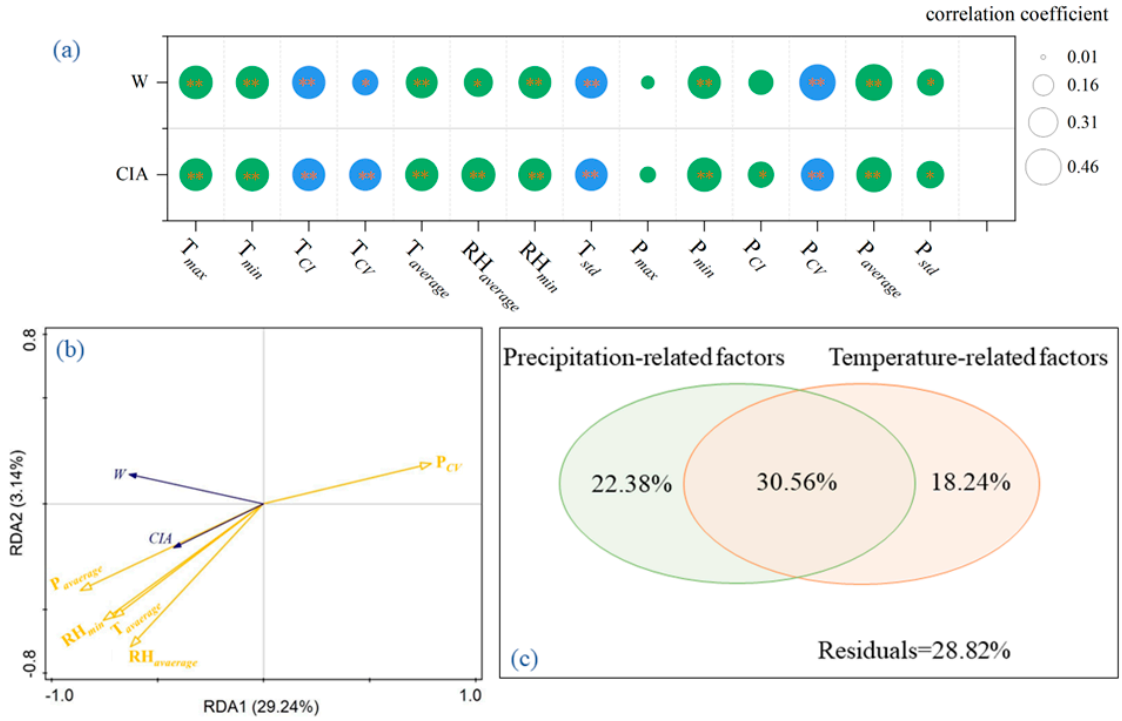

Figure 6. Correlation between granite weathering degree and climatic factors (**a**), ordination plot of redundancy analysis (RDA) for the granite weathering degree and climatic factors (**b**), and partitions of variation of granite weathering degree by climatic factors (**c**). T, P, and RH are temperature, precipitation, and relative humility, respectively; max, min, CI, CV, (max−min), average, and std denote the maximum, minimum, confidence interval, coefficient of variation, temperature difference between the maximum and minimum values, average value, and standard deviation, respectively. The blue and green colors in (**a**) respectively indicate negative and positive correlations with the climatic factor, and the size of these circles means the value of the correlation coefficients. * and ** represent significance at $p < 0.05$ and $p < 0.01$ levels, respectively.

4. Discussion

4.1. Evolution of Geochemical Elements during Granite Weathering

The weathering process of granite results from the intricate interplay of various geological and environmental factors [47–49]. It is initiated by the emplacement of the granite body, proceeds with exposure to a humid subtropical or tropical climate, and culminates under an essentially continuous weathering episode within a tectonically stable background [50]. According to regional geology and paleoclimate literatures, granites in this study area formed at a similar geological period [51–53]. Following the intrusion of granite units, it was hypothesized that they underwent progressive exhumation towards the Earth's land surface. This process was attributed to regional tectonic uplift during the late Cretaceous to Cenozoic period, along with subsequent denudation processes occurring throughout the Yanshanian–Himalayan geological events. Herein, geochemical elements showed significant clustering features with similarities in the same climatic conditions, while the geochemical attributes of the weathering process manifested distinct characteristics in various climates [54,55]. Chemical elements underwent widespread mobilization and redistribution during weathering, with their evaluation facilitated through the mass transfer coefficient ($\tau_{i,j}$) [45]. Additionally, the $\tau_{i,j}$ for CaO, MgO, Na_2O, K_2O, and SiO_2 predominantly exhibited negative values in the residual soil horizons, signifying leaching relative to the parent rock. The leaching rates followed the order CaO > Na_2O > MgO > K_2O, with Fe_2O_3 exhibiting a positive $\tau_{i,j}$, indicating enrichment relative to the parent rock (Figure 3). Meanwhile, the leaching degrees of CaO, MgO, Na_2O, and K_2O gradually increased from fresh rock to residual soils, aligning with the chemical properties of alkali earth metal ions. Particularly, the leaching rates of CaO and Na_2O approached 100%, suggesting near-complete loss attributed to continuous plagioclase weathering (Figure 4). The variation in element migration within the soil profile was intricately linked to the retention and leaching of diverse elements, as well as significant mineral transformations in the weathering crust. Owing to diverse hydrothermal conditions, the leaching levels of individual elements fluctuated, resulting in distinct weathering stages for the crust [3]. Herein, the concentration of ions in granite residual soil within the temperate region surpassed that in the subtropical area, with a heightened enrichment of the Fe and Al elements (Figure 2). The granite residual soil profiles examined in this study pertained to the weathering stage characterized by siliconization and aluminization. The subtropic generally represented a soft and aluminum-rich weathering region, further accentuated by the formation of an Al portal, constituting an aluminum-rich crust consistent with the distribution of weathering crusts in China.

Granite weathering also resulted in the redistribution and enrichment of rare earth elements. While most of the granite weathering profiles in this study exhibited comparable normalized chondrite curves with a steeper 'V' from Sm to Gd and smooth patterns from Gd to Lu (Figure 5), the presence of highly enriched REEs and variations in Eu and Ce indicated that weathering processes contributed to the release of REEs into the solution [2]. HREEs had a greater tendency to form soil hydrates with inorganic anions, providing them with increased stability compared to LREEs. Consequently, HREEs were more stable in the soil profile. Additionally, HREEs were more prone to release from the profile, resulting in a larger loss of HREEs compared to LREEs [1]. The content of REEs in weathering layers was seen to be much greater than that in the parent rock [41]. The secondary enrichment of rare earth elements (REEs) during the weathering process could have been influenced by various factors, including climate, clay fraction, pH, soil organic matter, and clay minerals [40]. The distribution pattern was impacted, on the one hand, by the kind of parent rock and, on the other hand, by the weathering degree [3]. During this process, primary minerals within the granite matrix containing REEs initially underwent chemical weathering due to exposure to atmospheric agents and water [47]. As these minerals broke down, they released REEs into the soil solution. The released REEs could then undergo several fate processes, including adsorption, leaching, fractionation, and secondary mineral formation [48,55]. The enrichment of REEs during granite weathering

resulted from a combination of mineral dissolution, adsorption–desorption processes, fractionation, and secondary mineral formation [2]. Herein, similar parent rocks led to a consistent fractionation model, while decreasing pH levels resulted in an increased concentration of REEs from north to south across the study area (Figures 3 and 6).

4.2. Linkage between Granite Weathering and Gully Erosion

Chemical weathering and physical erosion synergize in the formation of soils and the shaping of landscapes [8]. Physical erosion processes may rely on the chemical breakdown of rock, while chemical weathering is contingent upon the accessibility of newly exposed mineral surfaces generated through physical erosion. This study focused on similar granite parent rocks, and the spatial variation in the weathering degree aligned with the increasing hydrothermal conditions from north to south across the study area. Hence, the spatial differentiation of the granite weathering degree was predominantly governed by climatic conditions, especially those related to the temperate zone (Figure 6).

According to previous studies, granitic soils with comparatively low aggregate stability are susceptible to soil erosion [56–58]. The inherent metastable structure characterized by aggregation contributes to the perplexing erosion and slope failure in granitic soil areas [59]. The loose structure of the granite weathering mantle serves as the material foundation for gully erosion in subtropical China. The thickness of granite residual soil is frequently utilized to assess the occurrence and severity of gully erosion [60]. Field investigations indicated that gully erosion in subtropical China was predominantly observed to concentrate on granite residual soils characterized by a thickness ranging from 20 to 50 m [19]. Apparently, gully erosion in granitic soil areas only occurred in subtropical regions and could be attributed to the restricted thickness of the weathering mantle in temperate regions. It is widely acknowledged that the weathering degree decreases progressively with the increase in profile depth [61]. This vertical heterogeneity was more pronounced in subtropical regions than in temperate ones, consequently, diminishing slope stability in granitic soils in the subtropical region [20]. Nevertheless, abundant rainfall and rainfall erosivity accelerated soil erosion in the subtropical region. Therefore, the hydrothermal condition in the subtropical region contributed to the erosion material foundation and driving force for gully formation in this region. Specifically, temperate-related factors determined gully erosion materials by controlling the chemical weathering of granite (Figure 6), while rainfall-related factors acted as the driving force for gully erosion [22]. Collectively, the gully landscape represented a dynamic balance between granite weathering and soil erosion.

5. Conclusions

This study delved into the geochemical characteristics of granite weathering profiles across temperate to subtropical regions in China. As hydrothermal conditions increased from north to south, soil pH exhibited a shift from neutral to acidic, accompanied by the leaching of major elements, such as K_2O, Na_2O, CaO, and MgO, alongside an enrichment of Al and Fe. Dominant 2:1-type clay minerals in the temperate region generally transitioned to 1:1-type minerals from temperate to subtropic. ∑REEs and LREEs displayed less significant variations across the study area, while HREEs exhibited a higher concentration in the subtropical region. Plagioclases primarily governed the weathering process in temperate regions, with the involvement of K-feldspar gradually increasing and eventually dominating the process from temperate to subtropic regions. Furthermore, the quantified granite weathering degree, assessed by the CIA and W, generally decreased with an increasing profile depth, but increased from north to south across the study area. Despite the consistent parent rock, the spatial variation in the granite weathering degree was significantly influenced by climate conditions, particularly the comprehensive effects of temperature and precipitation. The obtained results suggested that a subtropical climate is essential for the formation of erosion materials for gully erosion on granite weathering mantles. However, a further investigation is still needed to establish a quantitative relationship between granite weathering and gully erosion.

Supplementary Materials: The following supporting information can be downloaded at: https://www.mdpi.com/article/10.3390/w16050751/s1, Table S1: Basic information of study area. Table S2: Analysis methods for soil physicochemical properties. Figure S1: Location of the study sites along the climatic gradient across the East Asian monsoon region. FS, Fushun County in Liaoning Province; LY, Lingyi County in Shandong Province; QC, Qichun County in Hubei Province; GX, Ganxian County in Jiangxi Province; CT, Changting County in Fujian Province; WH, Wuhua County in Guangdong Province. Figure S2: Variations in physicochemical properties of granitic soils. Figure S3: Vertical variations in major elements are evident along the granite residual soil profiles. The red dot line represents the average element migration rate in the temperate zone, while the black dot line signifies the average element migration rate in the subtropic zone. The vertical line, positioned at a horizontal coordinate of 0, illustrates the migration rate of each element relative to its content in the parent rock. Figure S4: Regression analysis between plagioclase and Na_2O and CaO. Figure S5: Chondrite-normalized patterns of each REE fraction. Figure S6: Pearson correlation between REE fraction and soil physicochemical properties. References [62–67] are cited in the Supplementary Materials.

Author Contributions: Original, S.Z.; investigation and resources, Y.Z.; validation and data curation, G.H.; validation and methodology, B.Z.; review and editing, Y.L.; visualization and software, X.C.; data curation, J.X.; conceptualization, supervision, funding acquisition, and project administration, Y.W. All authors have read and agreed to the published version of the manuscript.

Funding: This research was supported by the National Natural Science Foundation of China (42277329; 41807065; 42077067), the Fundamental Research Funds for the Central Universities (2662021ZHQD003), and the China Postdoctoral Science Foundation (2018M640714).

Data Availability Statement: Some or all data, models, or code that support the findings of this study are available from the corresponding author and Supplementary Materials upon reasonable request.

Conflicts of Interest: Author Gang Huang was employed by the company Sichuan Energy Power Development Group Company Ltd. Bo Zhang was employed by the company Guangxi Nuclear Power Company Ltd. The remaining authors declare that the research was conducted in the absence of any commercial or financial relationships that could be construed as a potential conflict of interest.

References

1. Fu, W.; Li, X.; Feng, Y.; Feng, M.; Peng, Z.; Yu, H.; Lin, H. Chemical weathering of S-type granite and formation of Rare Earth Element (REE)-rich regolith in South China: Critical control of lithology. *Chem. Geol.* **2019**, *520*, 33–51. [CrossRef]
2. Ichimura, K.; Sanematsu, K.; Kon, Y.; Takagi, T.; Murakami, T. REE redistributions during granite weathering: Implications for Ce anomaly as a proxy for paleoredox states. *Am. Mineral.* **2020**, *105*, 848–859. [CrossRef]
3. Baldermann, A.; Dietzel, M.; Reinprecht, V. Chemical weathering and progressing alteration as possible controlling factors for creeping landslides. *Sci. Total Environ.* **2021**, *778*, 146300. [CrossRef]
4. Hong, D.; Wang, T.; Tong, Y. An outline about granitoids in China. *Geol. Rev.* **2007**, *53*, 9–16.
5. Niu, D. Research on the Environmental Factors and Erosive Mechanism of Collapsing Hill in South China. Ph.D. Thesis, Nanjing Forestry University, Nanjing, China, 2009.
6. Bourke, M.C.; Viles, H.A. *A Photographic Atlas of Rock Breakdown Features in Geomorphic Environments*, 1st ed.; Planetary Science Institute: Tucson, AZ, USA, 2007; p. 79.
7. Oliva, P.; Viers, J.; Dupré, B. Chemical weathering in granitic environments. *Chem. Geol.* **2003**, *202*, 225–256. [CrossRef]
8. Dixon, J.; Thorn, C. Chemical weathering and landscape development in mid-latitude alpine environments. *Geomorphology* **2005**, *67*, 127–145. [CrossRef]
9. Pope, G. Weathering in the tropics, and related extratropical processes. In *Treatise on Geomorphology*; Elsevier: Amsterdam, The Netherlands, 2022; pp. 279–298.
10. Liu, X.; Zhang, D.; Jia, Y. Soil physical properties of collapsing hill and gully and their indications for soil erosion: An example of Liantanggang collapsing hill and gully in Wuhua County of Guangdong. *Adv. Earth Sci.* **2013**, *28*, 802–811.
11. Liu, P.; Chen, R.; Wu, K.; Kang, X. Effects of Drying-Wetting Cycles on the Mechanical Behavior of Reconstituted Granite-Residual Soils. *J. Mater. Civil Eng.* **2020**, *32*, 04020199. [CrossRef]
12. Guo, T.; Wong, L.; Wu, Z. Microcracking behavior transition in thermally treated granite under mode I loading. *Eng. Geol.* **2021**, *282*, 105992. [CrossRef]
13. Bluth, G.J.S.; Kump, L.R. Lithologic and climatologic controls of river chemistry. *Geochim. Cosmochim. Acta* **1994**, *58*, 2341–2359. [CrossRef]
14. Zhao, L.; Ji, J.; Chen, J.; Liu, L.; Chen, Y.; Balsam, W.; Balsam, W. Variations of illite/chlorite ratio in Chinese loess sections during the last glacial and interglacial cycle: Implications for monsoon reconstruction. *Geophys. Res. Lett.* **2005**, *32*, 242257. [CrossRef]

15. Gingele, F.; De Deckker, P.; Norman, M. Late Pleistocene and Holocene climate of SE Australia reconstructed from dust and river loads deposited offshore the River Murray Mouth. *Earth Planet. Sci. Lett.* **2007**, *255*, 257–272. [CrossRef]
16. Buggle, B.; Glaser, B.; Hambach, U.; Gerasimenko, N.; Marković, S. An evaluation of geochemical weathering indices in loess-paleosol studies. *Quatern. Int.* **2011**, *240*, 12–21. [CrossRef]
17. Zhao, L.; Hong, H.; Fang, Q.; Yin, K.; Wang, C.; Li, Z.; Torrent, J.; Cheng, F.; Algeo, T. Monsoonal climate evolution in southern China since 1.2 Ma: New constraints from Fe-oxide records in red earth sediments from the Shengli section, Chengdu Basin. *Palaeogeogr. Palaeocl.* **2017**, *473*, 1–15. [CrossRef]
18. Xu, J. Benggang erosion: The influencing factor. *Catena* **1996**, *27*, 249–263.
19. Liao, Y.; Yuan, Z.; Zheng, M.; Li, D.; Nie, X.; Wu, X.; Huang, B.; Xie, Z.; Tang, C. The spatial distribution of Benggang and the factors that influence it. *Land Degrad. Dev.* **2019**, *30*, 2323–2335. [CrossRef]
20. Wei, Y.; Liu, Z.; Wu, X.; Zhang, Y.; Cui, T.; Cai, C.; Guo, Z.; Wang, J.; Cheng, D. Can Benggang be regarded as gully erosion? *Catena* **2021**, *207*, 105648. [CrossRef]
21. Liu, X.; Zhang, X.; Kong, L.; Wang, G.; Liu, H. Formation mechanism of collapsing gully in southern China and the relationship with granite residual soil: A geotechnical perspective. *Catena* **2022**, *210*, 105890. [CrossRef]
22. Wei, Y.; Liu, Z.; Zhang, Y.; Cui, T.; Guo, Z.; Cai, C.; Li, Z. Analysis of gully erosion susceptibility and spatial modelling using a GIS-based approach. *Geoderma* **2022**, *420*, 115869. [CrossRef]
23. Xia, J.; Cai, C.; Wei, Y.; Wu, X. Granite residual soil properties in collapsing gullies of south China: Spatial variations and effects on collapsing gully erosion. *Catena* **2019**, *174*, 469–477. [CrossRef]
24. Wei, Y.; Wu, X.; Wang, J.; Yu, H.; Xia, J.; Deng, Y.; Zhang, Y.; Xiang, Y.; Cai, C.; Guo, Z. Identification of geo-environmental factors on Benggang susceptibility and its spatial modelling using comparative data-driven methods. *Soil Till. Res.* **2021**, *208*, 104857. [CrossRef]
25. Zhang, X.W.; Kong, L.W.; Yin, S.; Chen, C. Engineering geology of basaltic residual soil in Leiqiong, southern China. *Eng. Geol.* **2017**, *220*, 196–207. [CrossRef]
26. Kirk, P.; Campbell, S.; Flecther, C.; Merriman, R. The significance of primary volcanic fabrics and clay distribution in landslides in Hong Kong. *J. Geol. Soc.* **1997**, *154*, 1009–1019. [CrossRef]
27. Wen, B.; Duzgoren-Aydin, N.; Aydin, A. Geochemical characteristics of the slip zones of a landslide in granitic saprolite, Hong Kong: Implications for their development and microenvironments. *Environ. Geol.* **2004**, *47*, 140–154. [CrossRef]
28. Aydin, A. Stability of saprolitic slopes: Nature and role of field scale heterogeneities. *Nat. Hazard Earth Syst.* **2006**, *6*, 89–96. [CrossRef]
29. Zhang, X.W.; Kong, L.W.; Cui, X.L.; Yin, S. Occurrence characteristics of free iron oxides in soil microstructure: Evidence from XRD. SEM and EDS. Bull. Eng. *Geol. Environ.* **2016**, *75*, 1493–1503. [CrossRef]
30. Chen, J.; Zhou, M.; Lin, J.; Jiang, F.; Huang, B.; Xu, T.; Wang, M.; Ge, H.; Huang, Y. Comparison of soil physicochemical properties and mineralogical compositions between noncollapsible soils and collapsed gullies. *Geoderma* **2018**, *317*, 56–66. [CrossRef]
31. Dicenzo, P.D.; Luk, S.H. gully erosion and sediment transport in a small subtropical catchment, South China. *Catena* **1997**, *29*, 161–176. [CrossRef]
32. Liao, Y.; Yuan, Z.; Zhuo, M.; Huang, B.; Nie, X.; Xie, Z.; Tang, C.; Li, D. Coupling effects of erosion and surface roughness on colluvial deposits under continuous rainfall. *Soil Till. Res.* **2019**, *191*, 98–107. [CrossRef]
33. Jiang, F.; Huang, Y.; Wang, M.; Lin, J.; Zhao, G.; Ge, H. Effects of rainfall intensity and slope gradient on steep colluvial deposit erosion in southeast china. *Soil Sci. Soc. Am. J.* **2014**, *78*, 1741–1752. [CrossRef]
34. Liao, D.; Deng, Y.; Duan, X.; Cai, C.; Ding, S. Variations in weathering characteristics of soil profiles and response of the Atterberg limits in the granite hilly area of South China. *Catena* **2022**, *215*, 106325. [CrossRef]
35. Wang, K.; Wang, H.; Shi, X.; Weindorf, D.; Yu, D.; Liang, Y.; Shi, D. Landscape analysis of dynamic soil erosion in Subtropical China: A case study in Xingguo County, Jiangxi Province. *Soil Till. Res.* **2009**, *105*, 313–321. [CrossRef]
36. Liu, X.; Zhang, X.; Kong, L.; Wang, G.; Liu, H. Chemical weathering indices and how they relate to the mechanical parameters of granite regolith from southern China. *Catena* **2022**, *216*, 106400. [CrossRef]
37. Wei, Y.; Wu, X.; Cai, C. Splash erosion of clay–sand mixtures and its relationship with soil physical properties: The effects of particle size distribution on soil structure. *Catena* **2015**, *135*, 254–262. [CrossRef]
38. Xia, D.; Deng, Y.; Wang, S.; Ding, S.; Cai, C. Fractal features of soil particle size distribution of different weathering profiles of the collapsing gullies in the hilly granitic region, south China. *Nat. Hazards* **2015**, *79*, 455–478. [CrossRef]
39. Wei, Y.; Cai, C.; Guo, Z.; Wang, J. Linkage between aggregate stability of granitic soils and the permanent gully erosion in subtropical China. *Soil Till. Res.* **2022**, *221*, 105411. [CrossRef]
40. Deng, Y.; Duan, X.; Ding, S.; Cai, C.; Chen, J. Suction stress characteristics in granite red soils and their relationship with the collapsing gully in south China. *Catena* **2018**, *171*, 505–522. [CrossRef]
41. Wei, Y.; Wu, X.; Xia, J.; Miller, G.A.; Cai, C.; Guo, Z.; Hassanikhah, A. The effect of water content on the shear strength characteristics of granitic soils in South China. *Soil Till. Res.* **2019**, *187*, 50–59. [CrossRef]
42. Longerich, H. Analysis of pressed pellets of geological samples using wavelength-dispersive X-ray fluorescence spectrometry. *X-ray Spectrom.* **1995**, *24*, 123–136. [CrossRef]
43. Chen, Z.; Chen, Z.; Bai, L. Rare earth element migration in gullies with different Dicranopteris dichotoma covers in the Huangnikeng gully group, Changting County, Southeast China. *Chemosphere* **2016**, *164*, 443–450. [CrossRef]

44. Sun, S.S.; McDonough, W.F. Chemical and isotopic systematics of oceanic basalts: Implications for mantle composition and processes. *Geol. Soc. Lond. Spec. Publ.* **1989**, *42*, 313–345. [CrossRef]
45. Brimhall, G.H.; Dietrich, W.E. Constitutive mass balance relations between chemical composition, volume, density, porosity, and strain in metasomatic hydrochemical systems: Results on weathering and pedogenesis. *Geochim. Cosmochim. Acta* **1987**, *51*, 567–587. [CrossRef]
46. Ceryan, S. Weathering indices for assessment of weathering effect and classification of weathered rocks: A case study from NE Turkey. *Earth Sci.* **2012**, 19–44. [CrossRef]
47. Nesbitt, H.; Young, G. Prediction of some weathering trends of plutonic and volcanic rocks based on thermodynamic and kinetic considerations. *Geochim. Cosmochim. Acta* **1984**, *48*, 1523–1534. [CrossRef]
48. Li, Y.H.M.; Zhao, W.W.; Zhou, M.F. Nature of parent rocks, mineralization styles and ore genesis of regolith-hosted REE deposits in South China: An integrated genetic model. *J. Asian Earth Sci.* **2017**, *148*, 65–95. [CrossRef]
49. Jin, L.; Ma, L.; Dere, A.; White, T.; Mathur, R.; Brantley, S.L. REE mobility and fractionation during shale weathering along a climate gradient. *Chem. Geol.* **2017**, *466*, 352–379. [CrossRef]
50. Anderson, S.P.; Dietrich, W.E.; Brimhall, G.H. Weathering profiles, mass-balance analysis, and rates of solute loss: Linkages between weathering and erosion in a small, steep catchment. *Geol. Soc. Am. Bull.* **2002**, *114*, 1143–1158. [CrossRef]
51. Deng, Y.; Xia, D.; Cai, C.; Wang, Q.; Lyu, G.; Ding, S. Simulation of water characteristic curve in the soil profile of the collapsing gully on granite area of South China based on the fractal theory. *Sci. Soil Water Conserv.* **2016**, *14*, 1–8.
52. Twidale, C.R.; Campbell, E.M. Pre-Quaternary landforms in the low latitude context: The example of Australia. *Geomorphology* **1995**, *12*, 17–35. [CrossRef]
53. Butt, C.R.M.; Lintern, M.; Anand, R.R. Evolution of regoliths and landscapes in deeply weathered terrain-implications for geochemical exploration. *Ore Geol. Rev.* **2000**, *16*, 167–183. [CrossRef]
54. Wakatsuki, T.; Matsukura, Y. Lithological effects in soil formation and soil slips on weathering-limited slopes underlain by granitic bedrocks in Japan. *Catena* **2008**, *72*, 153–168. [CrossRef]
55. Anand, R.; Paine, M. Regolith geology of the Yilgarn Craton, Western Australia: Implications for exploration. *Aus. J. Earth. Sci.* **2002**, *49*, 3–163. [CrossRef]
56. Gong, Q.; Deng, J.; Wang, C.; Wang, Z.; Zhou, L. Element behaviors due to rock weathering and its implication to geochemical anomaly recognition: A case study on Linglong biotite granite in Jiaodong peninsula, China. *J. Geochem. Explor.* **2013**, *128*, 14–24. [CrossRef]
57. Hu, R.; Oyediran, I.; Gao, W.; Zhang, X.; Li, H. "Plagioclase solution degree index": A new index to evaluate the weathering degree of granite. *B. Eng. Geol. Environ.* **2014**, *73*, 589–594. [CrossRef]
58. Feng, Z.; Wang, S.; Liu, X.; Luo, W.; Wang, Q. Micro-area transportation of residues: A style of forming the red weathering crusts of carbonate rocks. *Acta Geol. Sin-Engl.* **2007**, *81*, 127–138. [CrossRef]
59. Derakhshan-Babaei, F.; Nosrati, K.; Tikhomirov, D.; Christl, M.; Sadough, H.; Egli, M. Relating the spatial variability of chemical weathering and erosion to geological and topographical zones. *Geomorphology* **2020**, *363*, 107235. [CrossRef]
60. Furbish, D.; Fagherazzi, S. Stability of creeping soil and implications for hillslope evolution. *Water Resour. Res.* **2001**, *37*, 2607–2618. [CrossRef]
61. Zhou, Z.; Su, S.; Diao, Y.; Wang, Z.; Wang, J.; Zhao, H. Seismic response and failure characteristics of granite slope using large-scale shaking table test. *Rock Soil Mech.* **2022**, *43*, 4.
62. Gee, G.W.; Or, D. 2.4 Particle-size analysis. *Methods Soil Anal.* **2002**, *4*, 255–293.
63. ASTM. *Annual Book of ASTM Standards 2000: Soil and Rock*; American Society for Testing Materials: West Conshohocken, PA, USA, 2000; Volume 4.
64. Thomas, G.W. Exchangeable cations. In *Methods of Soil Analysis Part 2. Chemical and Microbiological Properties*, 2nd ed.; Page, A.L., Miller, R.H., Keeny, D.R., Eds.; Agronomy Monograph, 9. American Society of Agronomy; Soil Science Society of America: Madison, WI, USA, 1982; pp. 159–165.
65. Mehra, O.P.; Jackson, M.L. Iron oxide removal from soils and clays by a dithionite-citrate system buffered with sodium bicarbonate. *Clays Clay Miner* **1958**, *7*, 317–327. [CrossRef]
66. Walkley, A.; Black, I.A. An examination of the Degtjareff method for determining soil organic matter, and a proposed modification of the chromic acid titration method. *Soil Sci.* **1934**, *37*, 29–38. [CrossRef]
67. Jackson, M.L. *Soil Chemical Analysis*, 2nd ed.; University of Wisconsin: Madison, WI, USA, 1979.